Subwavelength grating racetrack resonator based ultrasensitive refractive index sensor

Lijun Huang[1,2,*], Hai Yan[1], Xiaochuan Xu[3,*], Swapnajit Chakravarty[3], Naimei Tang[3], Huiping Tian[2,*], Ray T. Chen[1,3,*]

[1]*Dept. of Electrical and Computer Engineering, The University of Texas at Austin, Austin, TX 78758, USA*
[2]*State Key Laboratory of Information Photonics and Optical Communications, School of Information and Communication Engineering, Beijing University of Posts and Telecommunications, Beijing 100876, China*
[3]*Omega Optics Inc., 8500 Shoal Creek Blvd., Austin, TX, 78759, USA*
**Corresponding author: hljnet@163.com, xiaochuan.xu@omegaoptics.com, hptian@bupt.edu.cn, chenrt@austin.utexas.edu*

Abstract: An ultrasensitive transverse magnetic mode subwavelength grating racetrack resonator with a sensitivity of 429.7nm/RIU and a detection of limit of 3.71×10^{-4} RIU is demonstrated experimentally.

OCIS codes: (160.5298) Photonic crystal; (130.5296) Photonic crystal waveguides; (130.6010) Sensors;

In recent decades, silicon-on-insulator (SOI) platform has been intensively investigated for point-of-care applications. A wide range of devices, such as two-dimensional photonic crystal (PhC) micro-cavity resonators [1, 2], one dimensional PhC nanobeam resonators [3, 4], and ring resonators [5] have been demonstrated. Ideally, these devices must have a high sensitivity and a low detection of limit, which are strongly limited by the optical loss, the light polarization, and the overlap of light and surrounding matter. Several approaches were proposed and demonstrated to enhance the photon-analyte interaction and sensitivity by confining light in the low refractive index region, such as ring slot resonators [6, 7], slot waveguides [8], and nano-holes [9]. Yet their detection of limit is poor due to the increase of loss. In this paper, subwavelength grating racetrack resonators are proposed and experimentally demonstrated, which can achieve high sensitivity and low detection of limit simultaneously.

The 3D schematic of the proposed SWGRTR is shown in Fig. 1(a). The magnified image between SWG waveguide and SWG racetrack waveguide is shown in Fig. 1(b). Λ is the period of the SWG structure and equals 200 nm. L, W, and H are the length, width and thickness of silicon (Si) pillars, respectively. L_c and G represent the coupling length and the gap between the SWG waveguide and racetrack waveguide, respectively. The radius of racetrack is 10μm. The thickness of the buried oxide is 3μm. The upper cladding is the analyte solution to be detected. TM mode profiles (RSoft 3D BandSOLVE simulations) on xy plane at different cutting positions (red and blue dash line in Fig. 1(b)) are shown in Figs. 1(c) and 1(d). The silicon duty cycle in this simulation is 0.7 and the dimension of the silicon pillar (L×W×H) is 140 nm×600nm ×220nm. The plot of the mode volume overlap factor in relation to the duty cycle and width of pillars is shown in Fig. 1 (e). The 39.7% overlap factor of TM modes is larger than the 30.2% of TE modes with the same size of pillars. Thus, compared to the TE mode SWGRTRs with the same geometry, a higher sensitivity for TM mode SWGRTRs is anticipated. Fig. 1(f) summarizes the correlation between coupling strength and coupling gap and length. The critical coupling condition can be satisfied when the gap is 140nm and the coupling length is approximately equal to 6μm according to the simulation.

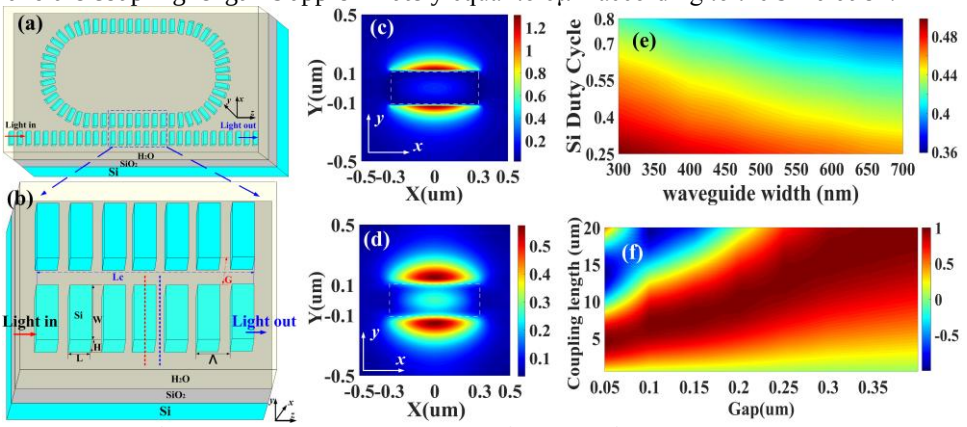

Figure 1. (a) The 3D schematic of the proposed SWGRTR. (b) The magnified image of the SWG bus waveguide and the SWG racetrack waveguide in rectangular region with a blue dash line. E_y electric fields of TM mode within silicon pillar to enhance light-matter interaction with L×W×H of 140 nm×600nm ×220nm in xy plane in red (c) and blue (d) dash line position in (b) around 1550 nm. (e) Plot of overlap of light and matter versus duty cycle and width of Si pillars. (f) Plot of coupling efficient changing with coupling length L_c and gap G around 1550 nm.

Fig. 2(a) is the scanning electron microscopy (SEM) image of the fabricated SWGRTR. Fig. 2(b) is SEM image of the TM mode grating coupler. Figs. 2(e) and 2(f) are the magnified SEM images of the left taper between strip waveguide and SWG waveguide, and the coupling region of the SWG bus waveguide and SWG racetrack waveguide, respectively. The fabricated SWGRTR is measured in DI water and the transmission spectrum is shown in Fig. 2 (c). The sensitivity of the proposed SWGRTR is calculated by monitoring resonance shift when different concentration solutions (0%, 5%, 10% and 20% glycerol) are consecutively injected onto the surface of the fabricated samples through microfluidic channels. The results are shown in Fig. 2(d). Fig. 2(g) shows the shift of transmission spectra after the new concentration solutions are injected. Fig. 2(h) is the plot of linear fitting of the resonance shift in relation to the change of refractive index of the solution. A bulk sensitivity of 429.7nm/RIU for the fabricated SWGRTR is achieved. The sensitivity of the fabricated SWGRTR, with a relative larger waveguide width (600 nm) and smaller radius of racetrack (10μm), is larger than 402nm/RIU in the SWG ring with the waveguide width of 500 nm and 30μm radius of ring, and the intrinsic detection limit (*iDL*) of the proposed structure is 3.71×10^{-4} RIU, lower than that in the ring resonator of 5.5×10^{-4} RIU [10]. The bulk sensitivity can be further improved by decreasing the Si duty cycle and the width of waveguide to increase the mode volume overlap.

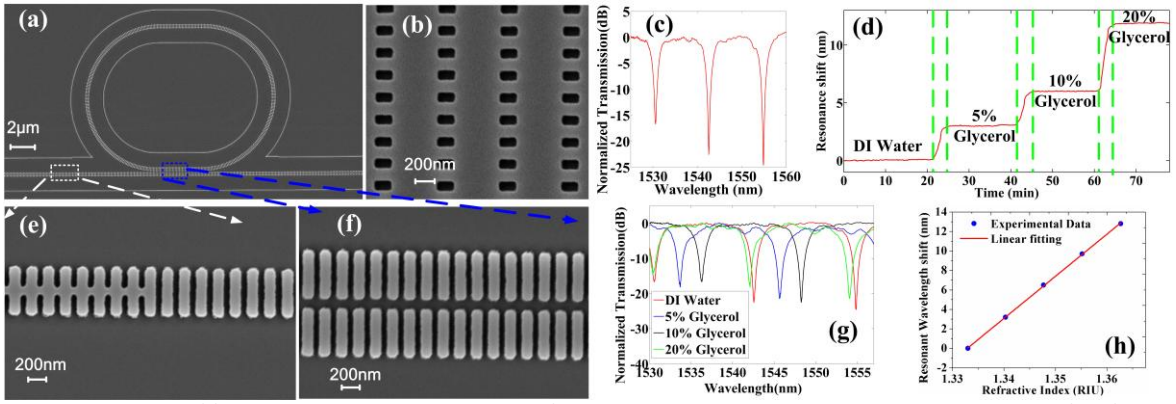

Figure 2. (a) SEM image of fabricated SWGRTR. (b) SEM image of the TM mode grating coupler. (c) Transmission spectrum of the fabricated TM mode SWGRTR in DI water. (d) Resonance shift for fabricated SWGRTR with different concentration glycerol solutions. The magnified SEM images of (e) the left taper between strip waveguide and SWG waveguide in white dash rectangular region, and (f) the coupling region between the SWG bus waveguide and racetrack waveguide in blue dash rectangular region. (g) Shift of the transmission spectra for different concentration glycerol solutions (0%, 5%, 10% and 20%). (h) Fitting plot of resonance shifts.

The research is supported by the Department of Energy Small Business Innovation Research (SBIR) program under the contract # DE SC-00113178. National Cancer Institute/National Institutes of Health (NCI/NIH) (Contract #: HHSN261201500039C). L. Huang acknowledges the support by National Natural Science Foundation of China (No. 61372038), Fund of State Key Laboratory of Information Photonics and Optical Communications (Beijing University of Posts and Telecommunications)-IPOC2015ZC02, China and Postgraduate Innovation Fund of SICE, BUPT, 2015. L. Huang acknowledges the China Scholarship Council (CSC) (NO. 201506470010) for scholarship support.

[1]. X. Fan, I. M. White, "Optofluidic microsystems for chemical and biological analysis," Nat. photonics 5, 591 (2011).
[2]. H. Yan, Y. Zou, S. Chakravarty, C. J. Yang, Z. Wang, N. Tang, D. L. Fan, R. T. Chen, "Silicon on-chip bandpass filters for the multiplexing of high sensitivity photonic crystal microcavity biosensors", App. Phys. Let. 106, 121103 (2015).
[3]. Q. Quan, P. B. Deotare, and M. Loncar, "Photonic crystal nanobeam cavity strongly coupled to the feeding waveguide," Appl. Phys. Lett. 96, 203102-1 (2010).
[4]. L. Huang, J. Zhou, F. Sun, Z. F, H. Tian, "Optimization of One Dimensional Photonic Crystal Elliptical-Hole Low-Index Mode Nanobeam Cavities for On-chip Sensing," J. Lightwave Technol. 34, 3496, 2016.
[5]. V. Donzella, A. Sherwali, J. Flueckiger, S. M. Grist, S. T. Fard, L. Chrostowski, "Design and fabrication of SOI micro-ring resonators based on sub-wavelength grating waveguides," Opt. Exp. 23, 4791 (2015).
[6]. L. Huang, H. Tian, J. Zhou, Q. Liu, P. Zhang and Y. Ji, "Label-free optical sensor by designing a high-Q photonic crystal ring–slot structure," Opt. Commun. 335, 73 (2015).
[7]. L. Huang, H. Tian, J. Zhou and Y. Ji, "Design low crosstalk ring-slot array structure for label-free multiplexed sensing," Sensors 14, 15658, (2014).
[8]. C. A. Barrios, "Optical slot-waveguide based biochemical sensor," Sensors 9, 4751 (2009).
[9]. S. Chakravarty, A. Hosseini, X. Xu, L. Zhu, Y. Zou, R. T. Chen, "Analysis of ultra-high sensitivity configuration in chip-integrated photonic crystal microcavity bio-sensors," Appl. Phys. Lett. 104, 191109 (2014).
[10]. S. Schmidt, J. Flueckiger, W. Wu, S. M. Grist, S. T. Fard, V. Donzella, P. Khumwan, E. R. Thompson, Q. Wang, P. Kulik, X. Wang, A. Sherwali, J. Kirk, K. C. Cheung, L. Chrostowski, D. Ratner, "Improving the performance of silicon photonic rings, disks, and Bragg gratings for use in label-free biosensing," Proc. SPIE 9166, 91660M (2014).